17. J. H. K. K. Hirschberg *et al.*, *Nature* **407**, 167 (2000).
18. D. Seebach *et al.*, *Helv. Chim. Act.* **83**, 2115 (2000).
19. B. Baumeister, S. Matile, *Chem. Commun.* **2000**, 913 (2000).
20. C. L. Nesloney, J. W. Kelly, *J. Am. Chem. Soc.* **118**, 5836 (1996).
21. H. L. Schenk, S. H. Gellman, *J. Am. Chem. Soc.* **120**, 4869 (1998).
22. S. R. Griffiths-Jones, M. S. Searle, *J. Am. Chem. Soc.* **122**, 8350 (2000).
23. J. J. L. M. Cornelissen, M. Fischer, N. A. J. M. Sommerdijk, R. J. M. Nolte, *Science* **280**, 1427 (1998).
24. A. L. Spek, *PLUTON. A Program for Plotting Molecular and Crystal Structures* (University of Utrecht, Utrecht, Netherlands, 1995).
25. P. J. H. M. Adams is acknowledged for synthetic contributions, R. P. Sijbesma for help in interpreting the PXRD data, and P. Samori for recording some of the AFM micrographs. This research was supported financially by the Council for Chemical Sciences of the Netherlands Organization for Scientific Research (CW-NWO).

3 May 2001; accepted 21 June 2001

Topochemical Polymerization of C_{70} Controlled by Monomer Crystal Packing

Alexander V. Soldatov,[1]*† Georg Roth,[3] Alexander Dzyabchenko,[4] Dan Johnels,[5] Sergei Lebedkin,[2] Christoph Meingast,[1] Bertil Sundqvist,[6] Miro Haluska,[7] Hans Kuzmany[7]

Polymeric forms of C_{60} are now well known, but numerous attempts to obtain C_{70} in a polymeric state have yielded only dimers. Polymeric C_{70} has now been synthesized by treatment of hexagonally packed C_{70} single crystals under moderate hydrostatic pressure (2 gigapascals) at elevated temperature (300°C), which confirms predictions from our modeling of polymeric structures of C_{70}. Single-crystal x-ray diffraction shows that the molecules are bridged into polymeric zigzag chains that extend along the *c* axis of the parent structure. Solid-state nuclear magnetic resonance and Raman data provide evidence for covalent chemical bonding between the C_{70} cages.

Understanding the formation and properties of three-dimensionally (3D) cross-linked C_{60} (*1–3*) and C_{70} (*4*) requires a detailed knowledge of structure and bonding in their precursors, high-pressure polymerized (hpp) fullerenes (*5–8*). However, with few exceptions (*9–11*), structural studies have been performed on polycrystalline hpp fullerenes, and powder diffraction data are of insufficient quality to resolve individual carbon atom positions and C–C bond lengths of the polymers. In this respect, knowledge of the structure of polymeric C_{70} is particularly interesting because it may be relevant to the not yet understood phenomenon of reversible amorphization induced in this material by high pressure (*12*).

Attempts to produce polymeric C_{70} have generally been inconclusive. Laser desorption mass spectra of thin films irradiated with ultraviolet (UV) light indicated the presence of molecular clusters, although infrared (IR) spectra remained unchanged (*13*). High-pressure treatment of C_{70} powder up to 7.5 GPa at temperatures up to 800°C also did not change its structure and vibrational properties (*14*). New features in IR (*15, 16*) and UV–visible (*15*) absorption spectra of polycrystalline C_{70} were observed after treatment at 5 GPa, 300°C (*15*) and 7.5 GPa, 250°C (*16*), but these features were attributed to the formation of C_{70} dimers, which were later produced, isolated in pure form, and characterized spectroscopically (*17*). However, the crystal structure of C_{140} also remains unknown. All of these uncertainties have frustrated further attempts to access the polymeric state of C_{70} and to address the problem of C_{70} polymerization in general.

To guide our experimental studies, we generated a series of plausible structural models for polymeric C_{70} (Table 1) using rigid zigzag chains as the structural units. We rejected some "hypothetical" polymeric structures from the analysis as energetically unrealistic, such as a fivefold helix extended along the ⟨111⟩ direction in a crystal with cubic packing (CP) or chains formed in close-packed planes via 2+2 cycloaddition between "equator" double bonds of C_{70}. For comparison, we also constructed crystal structures based on rigid, energetically favorable C_{140} (C_{2h} symmetry). The molecular structure as well as the initial packing [either CP or hexagonal packing (HP)] were assumed to be similar to that in a monomer (*18–21*). The positions and mutual orientations of chains and dimers were then optimized via minimization of the lattice energy with a method (*22*) that successfully predicted the crystal structures of monomeric C_{60} and C_{70} and of polymeric C_{60}. The predicted structures (Table 1) show that, whereas dimers can be formed in either packing, a polymeric chain structure with a reasonably low free energy is possible only in hexagonal C_{70}, because CP does not have a symmetry element (twofold screw axis) required to build a polymer. We therefore decided to use a HP C_{70} single crystal as source material for high-pressure synthesis of a C_{70} polymer. The predicted polymeric structures were further used as starting models in the structure determination from our diffraction data (see below).

The single crystals of C_{70} were grown with a method described in (*23*) and were treated

Table 1. Predicted and observed crystal packings of C_{70} polymer and dimer (*26*). The observed monomer structure is from (*21*), *Z* is the number of fullerenes per unit cell, and the van der Waals lattice energy (per one C_{70}) was minimized with the Lennard-Jones 6-12 atom-atom potential with parameters r_0 = 3.7 Å, ε = −0.072 kcal/mol for carbons using the program PMC (*22*). ND, not determined.

	Monoclinic dimer	Trigonal dimer	Orthorhombic polymer	Hexagonal polymer	Observed polymer	Observed monomer
Space group	*C2/m*	*P*3_1	*Ccmm*	*P*6_3*/mcm*	*Ccmm*	*Pnam*
Z	4	6	4	6	4	4
Crystal packing	HP	CP	HP	HP	HP	HP
Lattice energy (kcal/mol)	−43.3	−42.8	−60.90	−51.64	ND	ND
Density (g/cm³)	1.844	1.835	1.916	1.736	1.804	1.733
Lattice parameters						
a (Å)	16.93	9.97	16.95	18.13	17.30	17.35
b (Å)	10.06	9.97	10.13	18.13	9.99	9.84
c (Å)	17.86	53.01	16.97	16.97	17.92	18.34
α (degrees)	90	90	90	90	90	90
β (degrees)	84.3	90	90	90	90	90
γ (degrees)	90	120	90	120	90	90

---

[1]Institut für Festkörperphysik, [2]Institut für Nanotechnologie, Forschungszentrum Karlsruhe–Technik und Umwelt, Post Office Box 3640, D-76021 Karlsruhe, Germany. [3]Institut für Kristallographie der Rheinisch-Westfälische Technische Hochschule Aachen, Jägerstrasse 17–19, D-52056 Aachen, Germany. [4]Karpov Institute of Physical Chemistry, 103064 Moscow, Russia. [5]Department of Chemistry, [6]Department of Experimental Physics, Umeå University, S-901 87 Umeå, Sweden. [7]Institut für Materialphysik, Universität Wien, A-1090 Wien, Austria.

*Present address: Department of Physics, Lyman Laboratory, Harvard University, Cambridge, MA 02138, USA.

†To whom correspondence should be addressed. E-mail: soldatov@physics.harvard.edu

under high pressure in a piston-and-cylinder device, with silicon oil as the pressure-transmitting medium. The crystals were annealed for 11 hours at 2 GPa and 300°C; the samples were then rapidly cooled to room temperature under pressure before pressure was slowly released. Unpolarized Fourier transform (FT)–Raman and IR absorption measurements were carried out at room temperature on a Bruker Equinox 55S spectrometer. After treatment, several of the Raman modes of pristine C_{70} had split and/or shifted from their original positions, some modes (at 260, 456, 701, and 737 cm^{-1}) disappeared, and new modes appeared (Fig. 1). The mode at 1564 cm^{-1} split into two new components at 1549 and 1572 cm^{-1}. Similarly, the FTIR spectrum of the same sample exhibited, for example, new modes at 512 and 524 cm^{-1} and characteristic patterns at 766 to 784 and 1414 to 1443 cm^{-1}. These spectral features were not observed for the ordered monomer phases of C_{70} and are therefore attributed to the symmetry lowering and distortion of the C_{70} molecule as a result of polymerization. The appearance of low-energy "intercage" Raman modes at 105 and 121 cm^{-1} indicates that covalent bonds formed between the molecules. The observed frequencies differ from the corresponding modes (89, 118, and 129 cm^{-1}) of C_{140} (*17*) and scale well with the analogous vibrations in the chain polymer (*24*) of C_{60}, providing additional evidence for the polymeric nature of the material produced.

The material survived the high-pressure treatment in single-crystalline form. The quality of the treated crystal was sufficient to collect a total of 2299 reflections (1661 with $|F| > 4\sigma|F|$, data up to $2\theta = 32.7°$) at 293 and 100 K on an imaging plate x-ray diffractometer with Mo K_{α} radiation. All reflections could be indexed with a pseudo-hexagonal cell with $a_{hex} = 9.99 \pm 0.01$ Å, $c_{hex} = 17.92 \pm 0.02$ Å. Figure 2 shows example images from the complete diffraction data set. As the symmetry of the C_{70} molecule and the site symmetries in the hexagonal lattice are incompatible, the crystal structure of the polymer is pseudo-symmetric with a unit cell of lower symmetry mimicking a hexagonal cell via multiple (pseudo-merohedric) twinning.

The polymer C_{70} data consequently resisted any attempt to determine the structure by "classical" crystallographic methods. It was therefore solved ab initio by global optimization using a systematic stepwise orientational and translational search routine. Optimization was performed in space group *P*1 with a re-indexed, pseudo-hexagonal data set that properly accounted for the symmetry reduction and the multiple twinning. After refinement, the model was subjected to a symmetry analysis (*25*) that resulted in a structure in the space group *Ccmm* (group 63) with four molecules in an orthorhombic unit cell with $a_o = 17.30 \pm 0.02$ Å, $b_o = 9.99 \pm 0.01$ Å, $c_o = 17.92 \pm 0.02$ Å. Eighty-two parameters were further refined, including threefold pseudo-merohedric twinning, without constraints or restraints (*26*). We stress that the orthorhombic polymer model from the energy optimization (Table 1) used as a starting point for the structure refinement converged to exactly the same result in an independent test if we permitted relaxation of carbon atom positions. This finding additionally emphasizes the adequacy of the predicted structural model.

The directions of the orthorhombic and pseudo-hexagonal (parent hexagonal monomer) axes are related as follows: $a_o = 2a_{hex} + b_{hex}$; $b_o = b_{hex}$; $c_o = c_{hex}$. Expressed in the pseudo-hexagonal cell at 100 K, polymerization corresponds to a shrinking of the lattice parameter *c* by 3.3% while the *a* parameter decreases by only 0.3% from its monomer value. The volume decreases by 4% with respect to the monomer (*21*). The structure (Fig. 3) is built from polymeric zigzag chains extended along the *c* axis of the parent hexagonal monomer structure. Neighboring molecules are linked via four-mem-

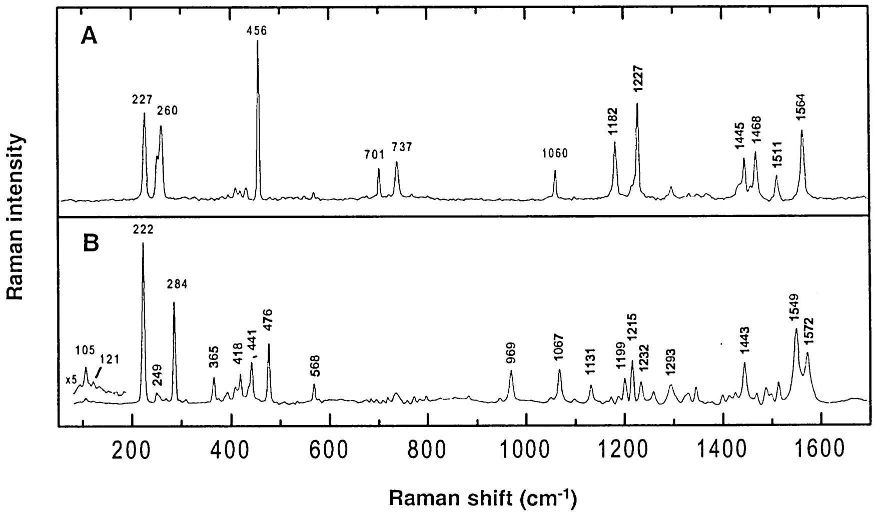

Fig. 1. Raman spectra of C_{70} single crystal (**A**) before and (**B**) after treatment at 2 GPa and 300°C for 11 hours.

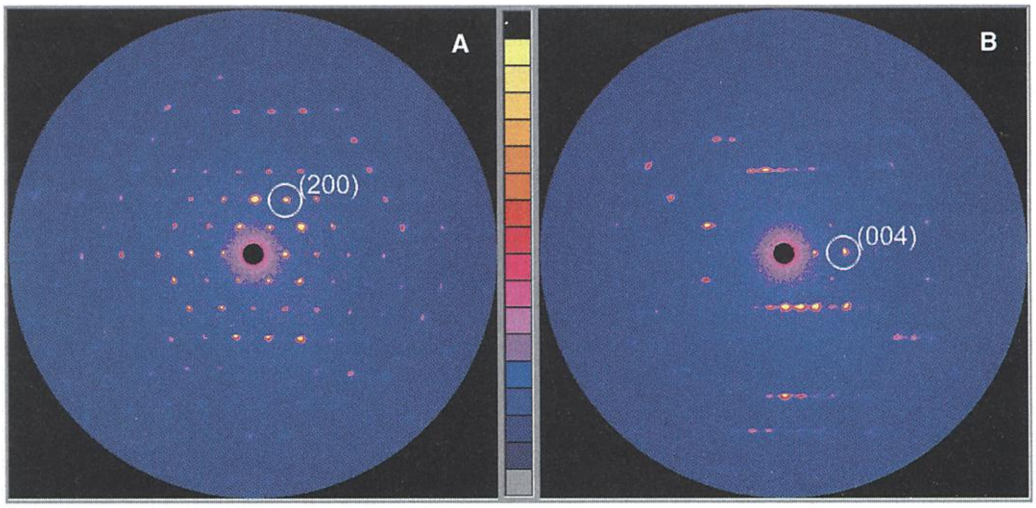

Fig. 2. Single frames from the imaging plate detector containing (**A**) the $(hk0)_{hex}$ plane and (**B**) the $[00l]_{hex}$ direction (pseudo-hexagonal notation) of the reciprocal lattice of the C_{70} polymer crystals. Characteristic reflections are encircled. The center of the image corresponds to $2\Theta = 0°$, the rim to $2\Theta = 32.7°$. The crystal was rotated around a vertical axis by 0.7° during exposure to collect integrated intensity data. Diffraction intensities increase from blue to yellow; higher intensities are cut off to better show the diffuse scattering. The pseudo-hexagonal metric is evident from (A). In (B), elongation of reflections and the pronounced diffuse scattering along c^*_{hex} indicates a high concentration of stacking faults in planes perpendicular to c_{hex}.

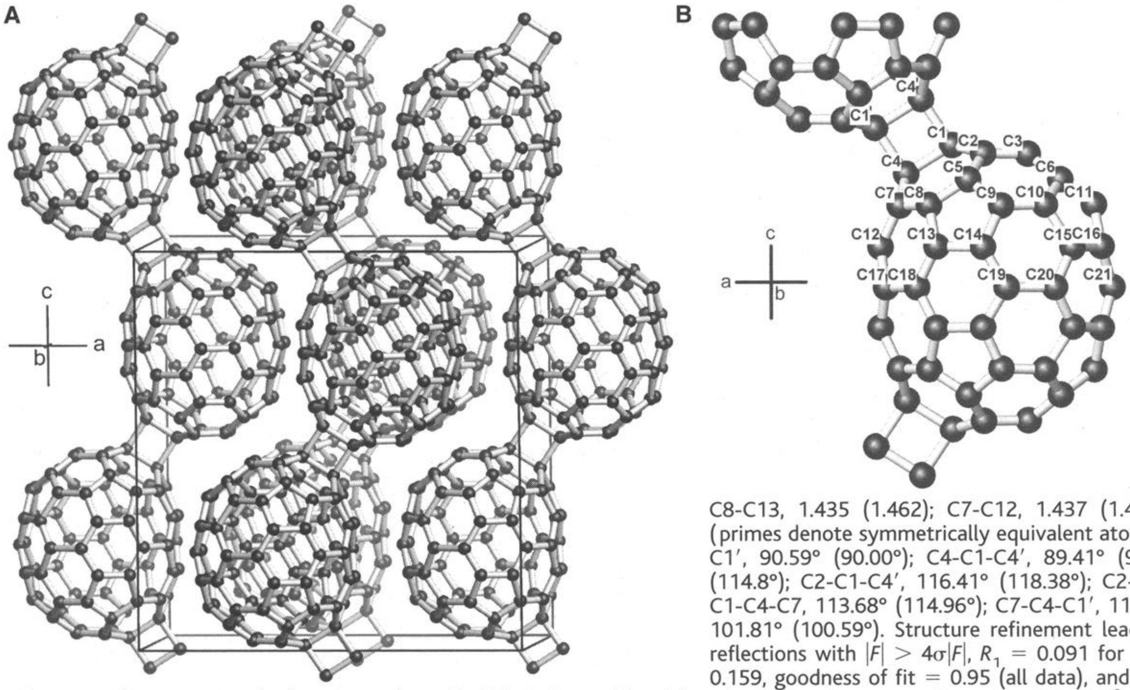

Fig. 3. Crystal structure of C_{70} polymer with unit cell shown in a 3D view (**A**) and an individual C_{70} molecule from the chain and a part of the neighboring cage closest to the four-membered ring (**B**). In the following, values in parentheses are calculated values for C_{140}. Selected bond lengths (Å): C1-C4, 1.625 (1.548); C1-C4, 1.621 (1.600); C1-C2, 1.525 (1.517); C2-C5, 1.370 (1.374); C5-C8, 1.428 (1.469); C7-C8, 1.357 (1.358); C4-C7, 1.496 (1.514); C2-C3, 1.427 (1.442); C5-C9, 1.438 (1.448); C8-C13, 1.435 (1.462); C7-C12, 1.437 (1.453). Selected bond angles (primes denote symmetrically equivalent atoms in the molecule): C1-C4-C1', 90.59° (90.00°); C4-C1-C4', 89.41° (90.00°); C2-C1-C4, 115.80° (114.8°); C2-C1-C4', 116.41° (118.38°); C2-C1-C2', 103.50° (101.34°); C1-C4-C7, 113.68° (114.96°); C7-C4-C1', 118.81° (118.59°); C4-C7-C7', 101.81° (100.59°). Structure refinement leads to $R_1 = 0.066$ for 1661 reflections with $|F| > 4\sigma|F|$, $R_1 = 0.091$ for all 2299 reflections, $wR_2 = 0.159$, goodness of fit = 0.95 (all data), and $R_1 = 0.073$ for 511 unique reflections after averaging (*26*). Estimated standard deviations of bond lengths and angles are on the order of 0.005 Å and 0.4°, respectively.

Fig. 4. ^{13}C MAS NMR spectrum of C_{70} treated at 2.5 GPa, 300°C. The peak at 110.8 ppm (asterisk) is a background signal from the Teflon end caps, and the peak at 5 ppm is a spinning sideband (ssb).

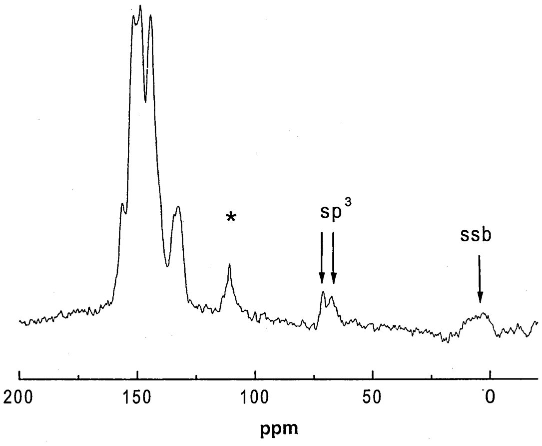

bered rings in a 2+2 cycloaddition between double bonds close to polar pentagons of the C_{70} cages. The pseudo-hexagonal crystal structure of the C_{70} polymer is indicative of the topochemical character of polymerization and suggests that the reaction takes place in a phase with uniaxial rotation of the molecules about their long axes, which are oriented along the *c* axis of the hexagonal lattice of the monomer (*27*). Hence, the alignment of molecules and their presumed orientational mobility would facilitate polymerization via spatial adjustment of reactive double bonds of neighboring cages.

The molecules in the chains are remarkably distorted, with elongated bonds and "flat" polygons on the "outer" surface of the chain links and short bonds and strongly nonplanar polygons on the "inner" surface, showing that polymerization results in very large molecular strains. The polygons close to the linking C atoms, in particular the polar cap pentagons, deviate most strongly from planarity. As expected, the polymerization-induced changes of the intramolecular bonds are largest close to the four-membered ring, an almost regular square [as in C_{120} (*10*)] fusing neighboring molecules. According to our nuclear magnetic resonance (NMR) results, the bonding state of both C1 and C4 carbons should be close to sp^3 (Fig. 3B). The former short [1.423 Å (*21*)] double bond, C1=C4, fusing two hexagons, is now the longest bond on the molecule (1.621 Å).

To compare our experimental results with quantum chemical predictions, we carried out the optimization of the geometry of the C_{70} dimer using the semi-empirical PM3 method [Gaussian 98W (*28*)]. The experimental data on the C_{70} polymer agree reasonably well with our predicted molecular bonds for the dimer, with most deviations in the range 0.02 to 0.03 Å (Fig. 3B). However, the intercage bonds C1-C4' and C4-C1' (1.548 Å predicted versus 1.625 Å observed) do not agree well. This deviation may be due to shortcomings of the quantum chemical approximation used here, because this highly strained part of the molecule is probably the most difficult to predict. However, in the case of incomplete polymerization and/or presence of stacking faults (Fig. 2B) terminating the growth of polymeric chains, one would expect an apparent elongation of these bonds that would result from a local relaxation of the molecules and a global increase of the lattice parameter along the chain. A rough estimate shows that the apparent difference of about 0.08 Å between the experimental intercage bond lengths for the polymer and those calculated for the dimer corresponds to about a 7% reduction in the degree of polymerization. This result is consistent with the fraction of C_{70} monomers (<5%) in the material estimated from the FTIR data. Quantum chemical calculations for infinite C_{70} chains would be needed to resolve this question.

In a ^{13}C magic angle spinning (MAS) NMR experiment, polymerized C_{70} in powder form, produced under similar conditions (2.5 GPa, 300°C) (*29*), was loaded into a 4.4-mm Chemagnetics pencil rotor and rotated at 14 kHz in a magnetic field of 9.4 T at room temperature. The NMR spectrum (Fig. 4) contains several resonances between 160 and 65 ppm (adamantane served as external reference). The two prominent signals at 67.6 and 71 ppm are typical of sp^3 carbons. As for polymeric C_{60} (*24, 30*), these signals are direct evidence for the formation of covalent bonds between molecules. More important, the two different chemical shifts of the sp^3 carbons directly confirm the results of our structural refinement—that is, the symmetry inequivalence of the two carbon atoms bridging neighboring molecules in the polymeric chains. Deconvolution of the spectrum in the sp^2 region between 130 and 160 ppm with Lorentzians reveals seven peaks, as compared to five peaks for the monomeric species, and is a further manifestation for cage deformation upon polymerization.

Although the C_{70} polymer crystal is stable at ambient conditions, it reverts to the monomeric state upon heating at ambient pressure, much like C_{60} polymers. Our dilatometric experiments on the single-crystal sample of the C_{70} polymer (*31*) indicate the onset of depolymerization as an abrupt increase of sample dimensions starting at about 450 K. Upon completion of this process, the orientational order-disorder transitions characteristic of molecular dynamics in the monomeric C_{70} are restored and the Raman spectrum of the material is identical to that of pristine C_{70} (Fig. 1A).

Our results demonstrate how nature solves the seeming problem of incompatible molecular (fivefold) and crystal (sixfold) symmetries of C_{70} by forming zigzag polymer chains. The topochemical polymerization is governed by the packing of molecules in C_{70} crystal and indicates that the system topology must play a key role in the polymerization of higher fullerenes and formation of 3D networks of cross-linked fullerene cages.

References and Notes

1. V. D. Blank *et al.*, *Phys. Lett. A* **205**, 208 (1995).
2. L. Marques *et al.*, *Science* **283**, 1720 (1999).
3. S. Okada, S. Saito, A. Oshiyama, *Phys. Rev. Lett.* **83**, 1986 (1999).
4. V. D. Blank *et al.*, *Phys. Lett. A* **248**, 415 (1998).
5. A. M. Rao *et al.*, *Science* **259**, 955 (1993).
6. Y. Iwasa *et al.*, *Science* **264**, 1570 (1994).
7. M. Nunez-Regueiro, L. Marques, J.-L. Hodeau, O. Bethoux, M. Perroux, *Phys. Rev. Lett.* **74**, 278 (1995).
8. B. Sundqvist, *Adv. Phys.* **48**, 1 (1999).
9. R. Moret, P. Launois, P.-A. Persson, B. Sundqvist, *Europhys. Lett.* **40**, 55 (1997).
10. G.-W. Wang, K. Komatsu, Y. Murata, M. Shiro, *Nature* **387**, 583 (1997).
11. R. Moret, P. Launois, T. Wågberg, B. Sundqvist, *Eur. Phys. J. B* **15**, 253 (2000).
12. N. Chandrabhas *et al.*, *Phys. Rev. Lett.* **73**, 3411 (1994).
13. A. M. Rao *et al.*, *Chem. Phys. Lett.* **224**, 106 (1994).
14. C. S. Sundar *et al.*, *Phys. Rev. B* **53**, 8180 (1996).
15. Y. Iwasa *et al.*, *Appl. Phys. A* **64**, 251 (1997).
16. M. Premila *et al.*, *Solid State Commun.* **104**, 237 (1997).
17. S. Lebedkin, W. E. Hull, A. Soldatov, B. Renker, M. M. Kappes, *J. Phys. Chem. B* **104**, 4101 (2000).
18. J. Baker, P. W. Fowler, P. Lazzeretti, M. Malagoli, R. Zanasi, *Chem. Phys. Lett.* **184**, 182 (1991).
19. G. B. M. Vaughan *et al.*, *Chem. Phys.* **178**, 599 (1993).
20. M. A. Verheijen *et al.*, *Chem. Phys.* **166**, 287 (1992).
21. S. van Smaalen *et al.*, *Chem. Phys. Lett.* **223**, 323 (1994).
22. A. V. Dzyabchenko, V. Agafonov, V. A. Davydov, *J. Phys. Chem. A* **103**, 2812 (1999).
23. M. Haluska *et al.*, *Appl. Phys. A* **56**, 161 (1993).
24. P. A. Persson *et al.*, *Chem. Phys. Lett.* **258**, 540 (1996).
25. L. Speck et al., *Program System PLATON* (Bijvoet Center for Biomolecular Research, University of Utrecht, Utrecht, Netherlands, 1999).
26. For supplementary data on parameter values, atomic coordinates, bond lengths, with further details of the refinement and modeling of polymeric and dimeric structures of C_{70}, see *Science* Online (www.sciencemag.org/cgi/content/full/293/5530/680/DC1).
27. A. Soldatov, B. Sundqvist, *J. Phys. Chem. Solids* **57**, 1371 (1996).
28. M. J. Frisch *et al.*, Gaussion 98W (Gaussian Inc., Pittsburgh, PA, 1998).
29. The FTIR spectrum of the powder material is similar to that of the single-crystal C_{70} polymer and indicates the fraction of C_{70} dimers less than 15%. The number of stacking faults in the powder is substantially larger than in the single crystal, which results in shorter polymeric chains. Nonetheless, this should not influence the characteristic features of the NMR spectrum of the polymer.
30. C. Goze *et al.*, *Phys. Rev. B* **54**, R3676 (1996).
31. A. Soldatov, P. Nagel, C. Meingast, unpublished data.
32. We thank S. Balibar, A. Bezryadin, E. Campbell, J. Fischer, Y. Iwasa, I. Silvera, and H. Suga for critical reading of the manuscript and valuable comments. A.S. gratefully acknowledges the Department of Physics, Umeå University, for support and for providing the experimental facilities for high-pressure synthesis. Further support is acknowledge from the Russian Foundation for Basic Research (A.D.) and by European Community project ERBFMRXCT970155 and Fonds zur Förderong de Wisenschaftlichen Forschung in Austria project P11943 (H.K.).

9 April 2001; accepted 15 June 2001

Calibration of the Lutetium-Hafnium Clock

Erik Scherer,* Carsten Münker, Klaus Mezger

Well-defined constants of radioactive decay are the cornerstone of geochronology and the use of radiogenic isotopes to constrain the time scales and mechanisms of planetary differentiation. Four new determinations of the lutetium-176 decay constant ($\lambda^{176}\mathrm{Lu}$) made by calibration against the uranium-lead decay schemes yield a mean value of $1.865 \pm 0.015 \times 10^{-11}$ year^{-1}, in agreement with the two most recent decay-counting experiments. Lutetium-hafnium ages that are based on the previously used $\lambda^{176}\mathrm{Lu}$ of 1.93×10^{-11} to 1.94×10^{-11} year^{-1} are thus ~4% too young, and the initial hafnium isotope compositions of some of Earth's oldest minerals and rocks become less radiogenic relative to bulk undifferentiated Earth when calculated using the new decay constant. The existence of strongly unradiogenic hafnium in Early Archean and Hadean zircons implies that enriched crustal reservoirs existed on Earth by 4.3 billion years ago and persisted for 200 million years or more. Hence, current models of early terrestrial differentiation need revision.

Estimates of the timing of dynamic processes in Earth and other planets are almost entirely based on radioactive decay systems that have half-lives between 10^5 and 10^{12} years. The Lu-Hf system, with a half-life of ~37 billion years, is both a versatile geochronometer and a powerful tool for studying the processes that control crust-mantle evolution. However, knowledge of the exact value of the decay constant for the β^--decay of $^{176}\mathrm{Lu}$ to $^{176}\mathrm{Hf}$ is vital to the correct interpretation of Lu-Hf data. The precision and accuracy of both Lu-Hf ages and initial Hf isotope compositions [$\varepsilon_{\mathrm{Hf}}(t)$, (*1*)] depend directly on $\lambda^{176}\mathrm{Lu}$. The first widely used Lu decay constant, $1.94 \pm 0.07 \times 10^{-11}$ year^{-1}, was derived from the slope of a Lu-Hf isochron for eucrite meteorites of known age (*2*, *3*). This value, based on age comparison, was used until 1997, when a more precise value [$1.93 \pm 0.03 \times 10^{-11}$ year^{-1}, (*4*)] obtained by decay counting was adopted (*5*). However, all other decay-counting experiments made since 1980 (*6*–*10*) yield lower values. The recommended (*10*) mean of recent decay-counting results, $1.86 \pm 0.01 \times 10^{-11}$ year^{-1} (*7*, *9*, *10*), is ~4% lower than both of the aforementioned decay constants. The accurate application of Lu-Hf systematics requires the reconciliation of decay constants determined from both decay-counting and age-comparison experiments.

Agreement between the two most recent decay-counting results (*9*, *10*) is due to the elimination of several experimental difficulties related to (i) optimizing detector geometry and calibration, (ii) knowing the exact amount of $^{176}\mathrm{Lu}$ in the sample, and (iii) correcting for the effects of gamma-ray attenuation, true-coincidence summing, and internal conversion (*10*). Age-comparison studies of minerals and rocks (*2*, *3*, *11*), in which $\lambda^{176}\mathrm{Lu}$ is calibrated against the relatively well-constrained U decay constants, have been limited by difficulties with measuring Hf isotope compositions and Lu concentrations by thermal ionization mass spectrometry (TIMS). Here, we measured Lu and Hf isotope ratios using multiple-collector inductively coupled plasma mass spectrometry

---

Institut für Mineralogie, Universität Münster, Corrensstrasse 24, 48149 Münster, Germany.

*To whom correspondence should be addressed. E-mail: escherer@nwz.uni-muenster.de